Turbulent Impurity Transport

Volker Naulin*, Jens Juul Rasmussen*, Clemente Angioni†, Carine Giroud**, Marco Valisa‡, Maria Ester Puiatti‡ and L. Carraro‡

*Association EURATOM-Risø- DTU, OPL-128, DK-4000 Roskilde, Denmark
†EURATOM-Association, MPI für Plasmaphysik, Garching D-85748, Germany
**EURATOM/UKAEA Fusion Association, Culham Science Centre, Abingdon, Oxfordshire OX14 3DB, United Kingdom
‡Consorzio RFX - Associazione Euratom-Enea sulla Fusione, I-35127 Padova,Italy

Abstract. Impurity transport is an important topic for ITER as impurity density in the core has to stay below a relative concentration of 5×10^{-5} [1] to reach ignition conditions. The reasons for that is mainly impurity radiation leading to cooling. In the edge region on the other hand site, higher impurity densities, going along with radiation energy losses are beneficial as the radiative cooling arranges for good power distribution onto the first wall.

Keywords: Impurities, turbulence, tokamaks, transport
PACS: 52.25.Vy,52.35.Ra,51.20.+d

INTRODUCTION

Thermonuclear fusion is easiest obtained using a mixture of Deuterium and Tritium as fuel. Any other material in the plasma diluting the fuel mixture is considered an impurity, this includes the Helium ash resulting from the fusion process. The Helium ash is, however, the only impurity species that has its source in the confined plasma region. All other impurities have their origin at the walls, from where they enter the plasma either as fast neutrals, originating from processes that release them from the walls, or they are already ionised in the scrape off layer, the SOL and transported across the last closed flux surface (LCFS) into the confined plasma region. Some impurities are deliberately injected into the plasma to influence the plasma properties in the SOL, for example to enhance the coupling of radiofrequency heating schemes, or are puffed or ablated, gaseous and solid impurities respectively, for transport experiments. In these cases the impurity sources are more or less known and we speak of extrinsic impurities. Materials that have their origin in the tokamak walls, either as material being deposited in layers onto the wall or wall materials themselves, are called intrinsic impurities. The sources of intrinsic impurities are badly known or not known at all.

Impurities influence the plasma performance through a number of processes. In the core the impurities dilute the plasma fuel, thus diminishing the efficiency of the fusion process. They can also influence through dilution the instabilities which drive transport and thus reduce core confinement. As impurities are usually materials with a rather high mass they efficiently radiate energy from the plasma and thus cool the plasma, an effect that is detrimental in the core, where high temperatures are needed to obtain fusion, but that is beneficial in the edge, where radiative cooling of plasma that leaves the confinement region. This distributes its energy onto a larger surface, compared to the rather small area that is "'wetted"' by the plasma flowing toward the divertor plates, which have to withstand tremendous heat fluxes. At the same time the presence of impurities can change the ratio between plasma density and temperature to obtain a certain critical plasma pressure at the edge, thus contributing to the H-mode physics as for example influencing the nature and frequency of edge localised modes (ELM) bursts, which pose one of the most difficult problems to obtain a technically viable operating regime for a fusion reactor.

This paper will discuss methods to investigate turbulent impurity transport only, classical and neoclassical impurity transport has been reviewed in detail in [2].

We will start by considering test particle transport in section two with a focus on simple and paradigmatic turbulence equations. A second part of these considerations will focus on the consistency of the test particle transport with bulk transport and the use of test particle densities instead of the particles themselves. The third paragraph we will describe different pinch effects, as they are of utmost importance in understanding peaked impurity profiles. Most of these pinches arrive due to finite compressibility of the advecting velocity field, with the best known being the curvature pinch originating in the compressibility of the velocity field perpendicular to the magnetic field direction, others

CP1013, *Turbulent Transport in Fusion Plasmas, First ITER International Summer School*
edited by S. Benkadda

pinch effects arising due to parallel velocity compressibilties and finally pinch effects from off -diagonal elements of the transport matrix, for example thermodiffusion, where the upgradient transport of particles is a consequence of a potentially large down gradient energy flux.

TEST PARTICLE TRANSPORT

Impurities in a plasma are never passive in the sense that they would not alter the stability of the plasma or details of the turbulence, they always participate in transport of heat, particles and momentum. However, it is a useful and instructive simplification to neglect theirinfluence on the bulk plasma and consider the impurities as species that are moved and changes by the plasma conditions around them, but exert no backreaction. Specifically, and besides energy losses through impurity radiation, this means that the impurity charge density plays only a negligible role in the quasineutrality condition expressed as $\nabla \cdot \vec{J} = 0$. The impurity contribution to quasineutrality must everywhere be smaller than each of the terms contributing to the quasi-neutrality condition from other species. Contributions to the quasi-neutrality are related to the fluctuating currents, which for an anomalous transport situation are brought about by the turbulence. Thus, a much more strict relationship has to be fulfilled, namely, the passive density must everywhere be smaller then the bulk current divergences building up in a characteristic time. For drift-wave like turbulence with a characteristic time given by ion larmor radius at electron temperature over ion sound speed ρ_s/c_s :

$$Z_{imp} n_{imp} \ll \rho_s/c_s \sum_{i,e} \nabla \cdot (n_s V_s) \,. \tag{1}$$

This is a strict condition, which cannot be guaranteed to be fulfilled in a real plasma at all times, as this would demand a correlation of the impurity densities with the bulk fluctuating quantities.

Noting that this condition will strictly not be fulfilled triggers an additional word of caution, if we consider self consistency. Let us make a "Gedankenexperiment" and assume we would be able to mark a certain number of bulk plasma ions, so that these marked ions fulfill the condition above. Obviously a short time after these particles have lost the memory of their starting positions, i.e., after a Lagrangian auto-correlation time, we expect and know that these particles are transported like the bulk plasma. They will be exhibiting the same gradient and the same relative flux. In fluid turbulence this allows to asses general transport properties of the turbulence from passive tracer dynamics [].

If passive tracers do not follow the bulk and do deviate from the bulk, then because the transport of passive test particles cannot tell us about f.x. the equilibrium pressure gradient. We would need the back reaction of the plasma density onto the fields governing its motion. Having stated this, we notice that the usual evaluation of anomalous transport in fluctuation based models does, however, not address the profile problem self-consistently as well. Consequently this approach will be able to to reveal pinch effects, but not self-consistently. On the positive side it has for a number of practical situations been shown, that the bulk transport and the one derived from the relative diffusion of passive test particles are indeed in agreement with each other [15, 16]. Deviations between passive tracer transport and bulk transport, as they appear, will only be resolved if we are able to solve the plasma profile problem for a multi-species plasma under turbulent action in a self-consistent manner.

Fundamentals of particle dispersion in turbulent flows

The classical results for particle dispersion in homogeneous turbulent flows dates back to the works of G.I. Taylor more than eighty years ago (see, e.g., [3, 4]). Here we present a short account of the basic features. Consider a particle released at $t = 0$ in an isotropic and homogeneous turbulent flow field characterized by the velocity fluctuations: $\vec{u}(\vec{x},t)$. The particle is assumed to ideally follow the flow as a passive tracer. The displacement of the particle from its initial position, which we may take to be the origin of the coordinate system without loss of generality, is determined as:

$$\vec{r}(t) = \int_0^t \vec{u}(\vec{r}(t'),t')dt',$$

where $\vec{v}(t) \equiv u(\vec{r}(t),t)$ designates the so-called Lagrangian velocity of the particle measured along its trajectory. The mean value of the displacement will be zero, since $\langle \vec{u}(\vec{r}(t),t) \rangle = 0$ (here $\langle \cdot \rangle$ denote average value). Thus, we shall consider the mean square displacement (the variance), which will be positive. The time derivative of the squared

displacement of the particle is calculated as follows:

$$\vec{r}(t)\frac{d}{dt}\vec{r}(t) = \frac{1}{2}\frac{d}{dt}(\vec{r}(t))^2 = \vec{v}(t)\cdot\int_0^t \vec{v}(t')dt' = \int_0^t \vec{v}(t)\cdot\vec{v}(t')dt'. \tag{2}$$

We now average this expression for the single particle over an ensemble of particles that are initialized all over the flow, and obtain the mean square displacement over the ensemble of particles: $R^2(t) \equiv \langle \vec{r}^2(t)\rangle$,:

$$\frac{dR^2(t)}{dt} = 2\int_0^t \langle \vec{v}(t)\cdot\vec{v}(t')\rangle dt'. \tag{3}$$

The integrand is expressed as

$$\langle \vec{v}(t)\cdot\vec{v}(t')\rangle = C_L(t-t')\langle v^2\rangle$$

where we have introduced the normalized Lagrangian autocorrelation function, C_L, for a time stationary turbulent flows (C_L depends only on the time differences) with $C_L(0) = 1$. $\langle v^2(t)\rangle$ is the mean square velocity fluctuations. (Note: for homogeneous turbulence the mean square of the Eulerian and Langragian velocity fluctuations are equal [3]). We define the Lagrangian integral time scale:

$$\tau_L \equiv \int_0^\infty R_L(\tau)d\tau,$$

which is a characterizing the memory of the dispersing particle. From Eq. 3 we obtain for the mean squared displacement:

$$R^2(t) = 2\langle v^2\rangle \int_0^t dt' \int_0^{t'} C_L(s)ds = 2\langle v^2\rangle \int_0^t (t-s)C_L(s)ds. \tag{4}$$

We may estimate $R^2(t)$ for two limiting cases:
i) short times $t \ll \tau_L$ where Eq. 4 reduce to

$$R^2(t) = 2\langle v^2\rangle t^2\,,$$

ii) long times $t \gg \tau_L$ where Eq. 4 reduce to

$$R^2(t) = 2Dt\,.$$

Thus, for short times the particle motion is ballistic, while for large times the dispersion is characterized by a diffusive process like Brownian motion with the variance growing linearly in time, and the diffusion coefficient expressed as

$$D = \langle v^2\rangle \tau_L.$$

Thus, if the full Lagrangian statistics of the flow were known then the particle dispersion could in principle be calculated. Furthermore, if the integral of the Lagrangian autocorrelation function is finite, i.e., τ_L is finite, the dispersion process will asymptotically approach a normal diffusion process.

In addition, to the two asymptotic regimes discussed above there is a regime for intermediate times of anomalous dispersion characterized by

$$R^2(t) \propto t^\sigma$$

where $\sigma > 1$ is referred to as *superdiffusion*, and $\sigma < 1$ is referred to as *subdiffusion*. The time window of this intermidiate regime may in principle be arbitrary wide when τ_L tend to infinity. Typical values of σ found in numerical simulations of particle dispersion in two-dimensional turbulence lays in the region $1.3 < \sigma < 1.7$ [5, 6, 7]. Although it is believed that it is the intermittent trapping and de-trapping of particles in coherent vortical structures that is responsible for the anomalous dispersion, it has not been possible to find/predict a unified value of σ. Various attempts have been proposed to describe the anomalous dispersion, including stochastic models [7] and fractal kinetics [8, 9].

The Lagrangian statistics is in general not obtainable. From standard single point measurements one obtains the Eulerian statistics and the relation between Eulerian and Lagrangian statistics is not at all trivial. Numerous works have been devoted basically to derive the Lagrangian correlation from the Eulerian statistics, see e.g. [4]. For two dimensional homogeneous turbulence a particularly simple result was suggested [10] for the scaling between the Lagrangian and Eulerian correlation functions: $C_L(\beta t) \approx C_E(t)$ where $\beta < 1$ is a parameter and thus $\tau_L < \tau_E$. This result was tested numerically with good agreement. Other studies also aim at providing the scaling of the diffusion coefficient with the rms-value of the fluctuations [11], and the analytical predictions have been compared with diffusion

of particles in a synthesized wave field modelling the turbulence [12]. These investigations were generalized further [13] to cases of strong turbulence where the assumptions behind the Taylor result are breaking down. This regime may be characterized by the so-called Kubo number $K > 1$, where $K = \langle v^2 \rangle^{1/2} T_c / \lambda$, T_c is a typical correlation time and λ is the averaged spatial scale of the fluctuations. The Kubo number measures the averaged distance covered by a particle during the correlation time relative to the typical spatial scale of the fluctuations. The results can be summarized by the dependence of the diffusion coefficient on the Kubo-number: $D \propto K^{\alpha}$, with $\alpha = 2$ for $K \ll 1$ and $\alpha \approx 0.7$ for $K \gg 1$. The particle trapping is found to partly hinder the diffusion, introducing a regime of subdiffusion.

Particle dispersion in plasma turbulence

The results discussed above also apply to to cross field particle dispersion in low frequency turbulence in magnetized plasmas. Here the fluctuating electric field give rise a fluctuating velocity field with the $E \times B$ velocity being the main contribution. For an overview of turbulent diffusion in magnetized plasmas see the Monograph by Balescu [14].

We shall shall here discuss a specific an example of test particle dispersion in electrostatic plasma turbulence. We base our discussions on the well-known Hasegawa-Wakatani equations (HWE) [15] for plasma edge turbulence driven by the resistive drift wave instability:

$$\partial_t n + \partial_y \varphi + \{\varphi, n\} = -C(n-\varphi) + \mu_n \nabla^2 n \,, \tag{5}$$

$$\partial_t \nabla^2 \varphi + \{\varphi, \nabla^2 \varphi\} = -C(n-\varphi) + \mu_\varphi \nabla^4 \varphi \,, \tag{6}$$

where n and φ are the fluctuating part of the density and potential, respectively. $1/C = 1/k_\parallel^2 L_\parallel^2$ is the adiabaticity parameter and contains via the parallel scale length $L_\parallel = (L_n T_e / m_e c_s \nu_{ei})^{1/2}$ the parallel resistivity.

It is inherently assumed that only one mode, parallel to the homogeneous magnetic field $\vec{B} = B_0 \hat{z}$, is excited, and all differential operators work in the (x,y)-plane, $\{\varphi, \psi\} \equiv \hat{z} \times \nabla\varphi \cdot \nabla\psi = \frac{\partial \varphi}{\partial x}\frac{\partial \psi}{\partial y} - \frac{\partial \psi}{\partial x}\frac{\partial \varphi}{\partial y}$. The x-coordinate is identified as the radial direction and the y-coordinate the poloidal direction and the model covers a slab region of the plasma-edge in a toroidal device. The fluctuating $E \times B$ velocity is given as $\vec{u} = (u,v) = (-\frac{\partial \varphi}{\partial y}, \frac{\partial \varphi}{\partial x})$. The normalization scales are $\rho_s = c_s/\Omega_i$ for lengths perpendicular to the magnetic field and L_n/c_s for the times, where $c_s = \sqrt{T_e/m_i}$ is the sound-speed and $L_n = (\nabla n_0(x)/n_0(x))^{-1}$ is the length scale of the radial back-ground density gradient (along x). Potential- and density-fluctuations are normalized by (T_e/e) (ρ_s/L_n) and $n_0 \rho_s / L_n$, respectively. The electron-temperature is constant, and we assume cold ions. μ_n is designating a diffusivity and μ_φ is the viscosity. For convenience and without loss of generality we take $\mu_n = \mu_\varphi = \mu$.

The HWE Eqs. (5,6) are solved numerically on a double periodic domain by means of a de-aliased pseudo-spectral code for details see [16, 17, 18]. After the initial linear growth the system enters a saturated turbulent state, where the global statistical properties show little or no time dependence, nor any dependence on the initialization method.

To gain statistically relevant results a large number of particles, typically more then 10000, that are passively advected by the flow have to be considered. The particles are initialized at random positions uniformly over the domain, when the turbulence has reached the quasi-steady regime. The trajectories of the particle are found from:

$$\vec{r}(t) = \vec{r}_0 + \int_0^t \vec{u}(\vec{r}(t'), t') dt' \tag{7}$$

where $\vec{r}_0$ is the initial position of the particle and $\mathbf{u}$ the velocity. The principal component of $\vec{u} = (u,v)$ is the $E \times B$ velocity evaluated at the position of the particle from the electrostatic potential φ: $\mathbf{u}_E = (-\partial_y \varphi, \partial_x \varphi)$. This velocity is employed when tracking ideal "massless" particles for which inertia effects can be neglected. Inertial effects can be incorporated by adding the polarization drift, $\mathbf{u}_p$ to $\mathbf{u}_E$, which may be written in normalized form:

$$\mathbf{u}_p = -\zeta \left(\frac{\partial}{\partial t} + (\mathbf{v}_E \cdot \nabla) \right) \nabla \varphi, \tag{8}$$

where $\zeta = \frac{eM}{qm_i} \frac{\rho_s}{L_n}$, M and q are the mass and charge of the particle. For the background, singly ionized ions, with charge e and mass m_i, $\mathbf{u}_p$ is a very small correction since $\frac{\rho_s}{L_n}$ is on the order of 0.01 or less ($\rho_s = c_s/\Omega_{ci}$ and L_n is the density scale length). But for heavy ions (e.g., impurity ions, or alpha particles) it might become important. In the next section we briefly investigate the influence of the polarization drift correction on the dispersion properties and in particular the

diffusion of heavy ions. The specific feature of this velocity is that it is compressible in contrast to the $E \times B$ velocity which in a homogeneous magnetic field is incompressible $\nabla \cdot \vec{u}_{E\times B} = 0$. For compressible convection velocities we have the possibility of clustering of particles and particularly of pinching, as will be discussed in the next section.

For the cases discussed above we inherently assumed that finite Larmor radius effects (FLR) could be neglected. That is, the typical scale lengths of the fluctuations are much larger than the Larmor radius of the particles. This holds well for "cold" impurity particles in the edge region. However, for high energetic particles like fusion alphas, having a Larmor radius of few cm the finite Larmor radius effect is certainly important. Then in principle the particle trajectory have to be calculated applying the full Lorenz force:

$$\frac{du_i}{dt} = -\frac{q}{m}\frac{\partial \phi'}{\partial x_i} + \Omega_c \varepsilon_{ij} u_j; \;\; \frac{dx_i}{dt} = u_i; \;\; \varepsilon_{12} = -\varepsilon_{21} = 1, \varepsilon_{ii} = 0.$$

However, provide that the time scale of the turbulence is much slower than the gyro-motion one apply the standard gyrokinetic approach. That is averaging the potential over the gyro orbit of the particle, which results in the effective - gyro averaged potential - given by

$$\phi^G(\vec{r}) = \frac{1}{(2\pi)^2}\int_{-\infty}^{\infty} d\vec{k} \exp(i\vec{k}\cdot\vec{r})\phi(\vec{k})J_0(k\rho) \tag{9}$$

where $\phi(\vec{k})$ designates the Fourrier transform of the potential, J_0 is the Bessel function of zero order, and ρ is the Larmor radius of the impurity ion. The particles are advected by the gyro averaged $E \times B$ velocity obtained from $\phi^G(\vec{r})$.

In the case of weak turbulence one will intuitively expect that the FLR will limit the dispersion, since the particle is sampling over a varying E-field and therefore experiences and effectively smaller $E \times B$ drift. This is in agreement with results of [19] who investigated the influence of FLR on particle dispersion in drift wave turbulence, and the results of Krane et al [20]. However, recently it has been shown that for the limit of large Kubo numbers the effect of the FLR becomes less dramatic [21], and for Kubo numbers of around 10 FLR only a weak reduction of the dispersion results. Similar results are also found by [22, 23], who applied these results to explain the anomalous diffusion of fast ions originating from off-axis neutral beam injection in Asdex Upgrade [24].

Particle dispersion

First we consider a dense collection of particles initially located in a small domain around the center of the box, Fig. 1. Initially we observe a large dispersion in the radial direction (along x). After around 16 time units the poloidal diffusion starts to dominate, and at $T = 80$, the initially dense particle collection confined to an (x,y) symmetric part of the flow has been dispersed to an area in the flow that is roughly two times as long in the y direction as in the x direction.

To describe the diffusion of a large ensemble of particles we introduce the running diffusion coefficient. We split it into a radial and poloidal (x and y) component defined as

$$D_x(t) = \frac{X^2(t)}{2t}, \;\; D_y(t) = \frac{Y^2(t)}{2t}, \tag{10}$$

where $X^2(t) = \langle (x(t) - x(t=0))^2 \rangle$, $Y^2(t) = \langle (y(t) - y(t=0))^2 \rangle$ are the mean square displacements of particles in radial and poloidal direction. The brackets denote an average over all particles. For a diffusive process the running diffusion coefficient $D(t)$ reaches a time independent value D, as $X^2(t) \sim t$ holds. We should note that the running diffusion coefficients ia often defined as the differential $D(t) = \frac{1}{2}\frac{dR^2}{dt}$, which also approach a constant in the diffusive limit. Applying the classical Taylor result for particle dispersion in turbulent flows (see the Introduction) for the two components of D the asymptotic diffusion coefficients can be expressed as:

$$D_x = \langle u^2 \rangle \tau_L, \;\; D_y = \langle v^2 \rangle \tau_L, \tag{11}$$

Employing the estimated value of $\tau_L \approx 2-3$ and the values of the rms velocity fluctuations $\langle u^2 \rangle \approx 1.4$, $\langle v^2 \rangle \approx 1.1$, which are only weakly dependent of C we would expect: $D_x = 4-5$ and $D_y = 2-3$ almost independent of C.

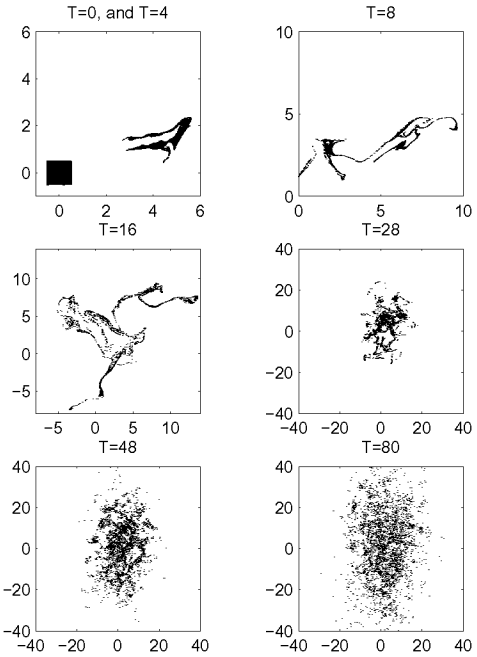

FIGURE 1. Dispersion of a dense sample of particles initially released in a square box at the center of the domain.

From the Lagrangian autocorrelation function we can estimate the Lagrangian integral time scale: $\tau_L = 2-3$, which is weakly dependent on C. Thus, the Kubo number, $K = \langle v^2 \rangle^{1/2} T_c/\lambda$, takes typical values of $K = 2-3$ for both radial and poloidal fluctuations, where the T_c is taken as τ_L and the averaged spatial scale length is estimated as $\lambda \sim 2$. Thus, the Kubo number is roughly constant for the parameters we have considered, and it is not possible to perform a Kubo number scaling of the dispersion properties.

In Fig. 2 we have shown the evolution of the radial and poloidal component of the running diffusion coefficient defined in (10) for different values of the coupling coefficient, C. We observe that D_x is strongly dependent on C, although it is found that $\langle u^2 \rangle$ only weakly decreased with C. After an initial ballistic phase, $D_x \propto t$, the coefficient decreases and finally tends to flatten out at least for $C \leq 2$. Thus, it appears that the evolution after a period of subdiffusive behaviour characterized by $X^2(t) \sim t^\sigma$ with $\sigma < 1$ approach an asymptotic diffusive regime, with a diffusion coefficient that is strongly decreasing with C. Indeed the diffusion is significantly smaller than the the "Taylor diffusion", Eq. (11). For the value $C = 5$ the subdiffusive behavior is more pronounced than at smaller C values. The poloidal diffusion is clearly larger than the radial one. For moderate values of C it is found to be in agreement with the value predicted from the Taylor-formula (11), however, for larger $C > 1$ it tends to increases with C with the tendency for superdiffusive behavior for large C-values ($C = 5$). This behavior and in particular the strong anisotropic effect for large C have also been observed for the dispersion of passive particles in the frame-work of the Hasegawa-Mima equation (see, e.g. [19, 25, 26].

The intermediate subdiffusive regime for the radial dispersion and the superdiffusive behavior for the poloidal dispersion was found to be related to trapping of particles in vortical structures [16]. A significant amount of particles are trapped in the vortical structures and convected with them for some time (typically t = 10 - 15 for moderate values of C). The vortical structures propagate predominantly in the poloidal direction with a poloidal velocity about 0.45, which is 3 times higher than their typical radial velocity 0.15. Thus, it may be estimated that the convection by the vortices will enhance the poloidal spreading and limit the radial spreading of the particles.

In order to investigate the radial subdiffusive and poloidal superdiffusive behavior in more detail for the case $C = 5$ we have plotted the mean square displacement both in radial and poloidal direction in Fig. 3a. For Y we observe a clear superdiffusive behavior in an intermediate time span ($5 < t < 100$), $Y^2 \sim t^\sigma$ with an exponent $\sigma \simeq 1.4$, while it is approaching a normal diffusion for $t > 100$ ($\sigma = 1$). For X it is more subtle, a naive fit would indicate a sub-

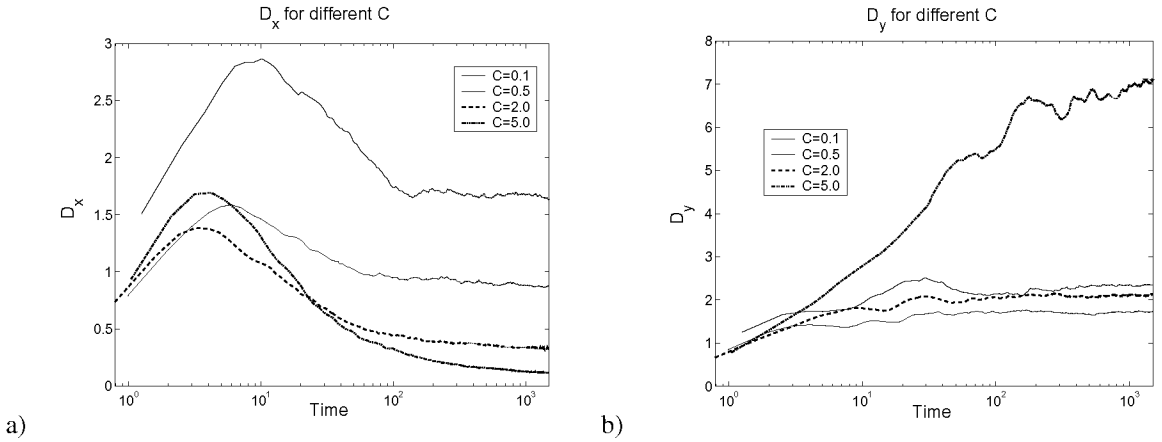

FIGURE 2. a) Running diffusion coefficient in the radial direction, D_x, and b) in the poloidal direction, D_y, versus time for various values of C.

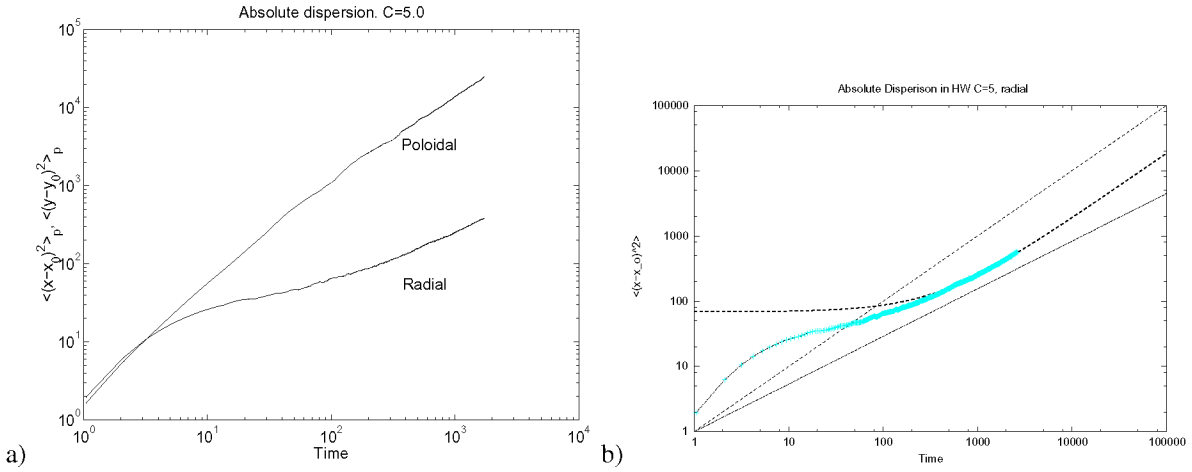

FIGURE 3. a) The mean square radial and poloidal particle displacement $X^2(t)$ and $Y^2(t)$ versus time for $C = 5$. For the radial displacement a subdiffusive regime is clearly visible for $t > 5$. For the poloidal/meridional displacement a superdiffusive regime is visible for $5 < t < 500$. b) A detailed fit to $X^2(t)$. The dashed curve is a least mean square fit of the form $At^\sigma + B$ to $X^2(t)$ for $t > 400$, where $\sigma = 1, A = 0.184, B = 68.75$. The dashed line has the slope 1 and the dot-dashed line has the slope 0.73.

diffusive behavior continuing for $t > 100$ with $X^2 \sim t^\sigma$, $\sigma \simeq 0.73$ following a stronger subdiffusive regime, $\sigma \simeq 0.5$, for $10 < t < 100$ However, a detailed fit, see Fig. 3b, shows that after the subdiffusive behavior for $10 < t < 500$ there is a a slow transition to the asymptotic diffusive behavior. The dashed curve is the best fit of a function of the form $At^\sigma + B$ for $t > 400$ with $\sigma = 1$. The "naive" fit in the regime $200 < t < 2000$, $X^2(t) \sim t^{0.73}$, is shown by the dot-dashes line.

Consistency with background transport

We would like to point out, that there are two ways to determine the plasma particle transport. One way is to determine the particle transport is to derive a diffusion coefficient from following passive tracer particles convected by the turbulent flow, as described above. The other way is to look directly at the convected density, leading to the familiar expression $\vec{\Gamma} = n\,\vec{u}_{E\times B}$ for the local turbulent particle flux. The radial component of $\vec{\Gamma}$ is the cross-field transport as usually measured in experiments and simulations of electrostatic turbulence, see e.g., [27, 28, 29, 30]. Note that an effective diffusion coefficient related to the flux is defined through Fick's law, $D^{eff} = \Gamma_0/\nabla n_0$, with our normalizations

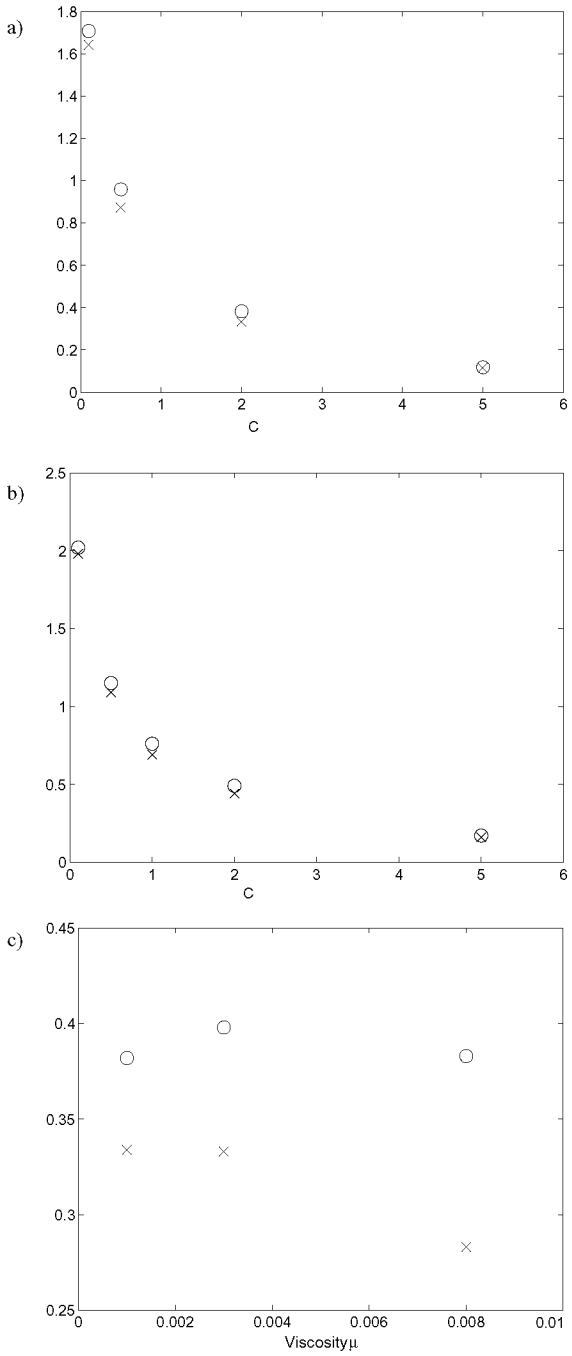

FIGURE 4. Comparison of radial diffusion coefficient D_x denoted by $\times$ and the diffusion coefficient obtained from the particle flux D_Γ (◯), for various values of C. a) Newtonian viscosity $\mu = 0.001$. b) Hyper-viscosity with the operator: ∇^6. c) For different values of the Newtonian viscosity and $C = 2$ (from [17]).

reduce to $D^{eff} = \Gamma_0$. Here Γ_0 is the flux averaged over the whole domain. A more elaborated discussion of the relation between the $E \times B$-flux and the particle diffusion is presented by [17]. Here we just show in Fig. 4 that the effective diffusion coefficient obtained from calculating the the mean flux and the particle diffusion coefficient are consistent. Thus for the present model with fixed and given density gradient the asymptotic diffusion coefficient for ideal tracers indeed is consistent with the transport of the bulk plasmas.

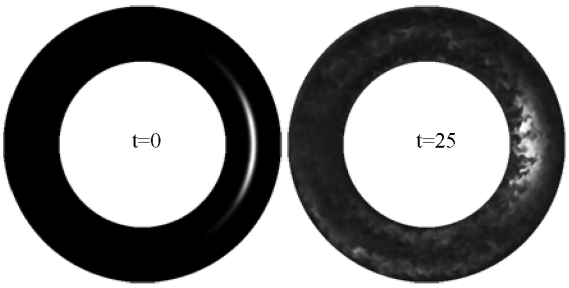

FIGURE 5. Poloidal crosssection showing impurity concentration initially (left) and after 25 time units (right) (from [35]).

DIFFERENT PINCH EFFECTS

Curvature pinch

The pinch effects may be generally ascribed to the compressibility of the advecting velocity field. As a simple example, we first consider a nonuniform magnetic field mimicking the toroidal field in toroidal devices, then the spatial dependence of the magnetic field will result in a compressibility of the $E \times B$ velocity $\nabla \cdot \vec{u}_{E\times B} = \hat{z} \times \varphi \nabla(1/B)$ for a simple slab geometry. The the pinch effect may simply be understood by considering the continuity equation for the impurity particle density N [31],

$$\left(\frac{\partial}{\partial t} + \frac{1}{B}\hat{z} \times \nabla\phi \cdot \nabla\right)\frac{N}{B} = 0, \tag{12}$$

which implies that N/B is a Lagrangian invariant advected by the compressible electric drift $\hat{z} \times \nabla\phi/B$. Now, assuming that the impurities are effectively mixed by the turbulent velocity fluctuations, this invariant will be uniformly distributed in space and the poloidally averaged impurity density $N_0(x)$ varies like $B(x)$. Thus, impurities released in the outboard midplane region will on average experience an inward transport, which corresponds to the the so-called inward pinch. This effect is usually referred to the curvature pinch, since the magnetic field inhomogeneity is originating from the curved toroidal geometry. The effect was clearly demonstrated in two-dimensional interchange instability simulations by employing the so-called ESEL code [32], and it was observed that impurities originating far out in the scrape-off-layer effectively was transported across the last closed flux surface and into the main plasma [33]

In a three dimensional flux tube geometry the curvature pinch was also clearly demonstrated for the transport of impurities in drift-Alfvén turbulence by employing the TYR code [34, 35]. Fig. 5 shows the poloidal projection of the impurity density development in that case. The analysis is based on expressing the flux Γ of the impurity species by the standard parameters used in modeling and in evaluation of transport experiments: a diffusion coefficient D and a convection velocity V, which is associated to a pinch effect:

$$\Gamma(s) = -D(s)\partial_x < n >_y + V(s) < n >_y . \tag{13}$$

The turbulence is radially homogeneous, so there is no radial dependence of D and V. Profiles $< \cdot >_y$ are obtained by averaging over y, corresponding to averaging toroidally over the domain extend in the drift plane, with s representing the coordinate along the magnetic field projected onto the poloidal plane. It is readily observed that by rewriting Eq. 13 in the form:

$$\Gamma(s)/ < n >_y = -D(s)\partial_x < \ln n >_y + V(s), \tag{14}$$

scatter plots of $\Gamma(s)/ < n >_y$ versus $\partial_x < \ln n >_y$ will provide values for $D(s)$ and $V(s)$. Figure 6 shows a scatter plot with a fit, and from the slope we obtain the value of D, while V is given by the offset at zero gradient. A comparison of the evolution of the impurity density profile with its presumed evolution using the values for D and V obtained from the above analysis is shown in Figure 7. This shows that while the scatter plot has a significant amount of noise, the fitted values for D and V are reasonably represents the overall transport process. Directly using such a kind of fit, would be an alternative method to determine the D and V values.

The dependence of D and V on s) is significant and as shown in Fig. 8. The effective convection velocity $V(s)$ changes sign and is at the high field side directed out of the plasma ($V(s)$ is directed towards the symmetry axis of the torus for all s). This pinching velocity is due to curvature and can be consistently explained within the framework of

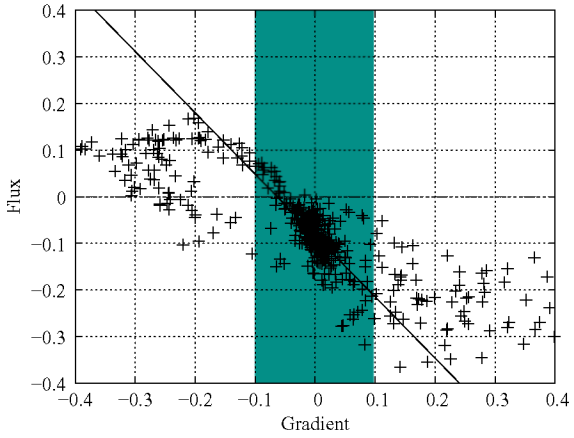

FIGURE 6. Scatter plot (at high field side) of flux versus gradient with linear fit, gray area indicates gradients admissed for the fitting procedure(from [35]).

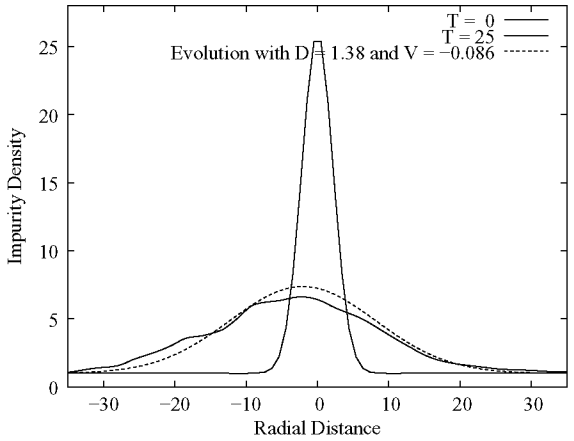

FIGURE 7. Impurity density profile at the outboard midplane at $t = 0$ and after 25 time units compared to the expected evolution of a Gaussian due to coefficients D and V obtained by the fitting procedure (from [35]).

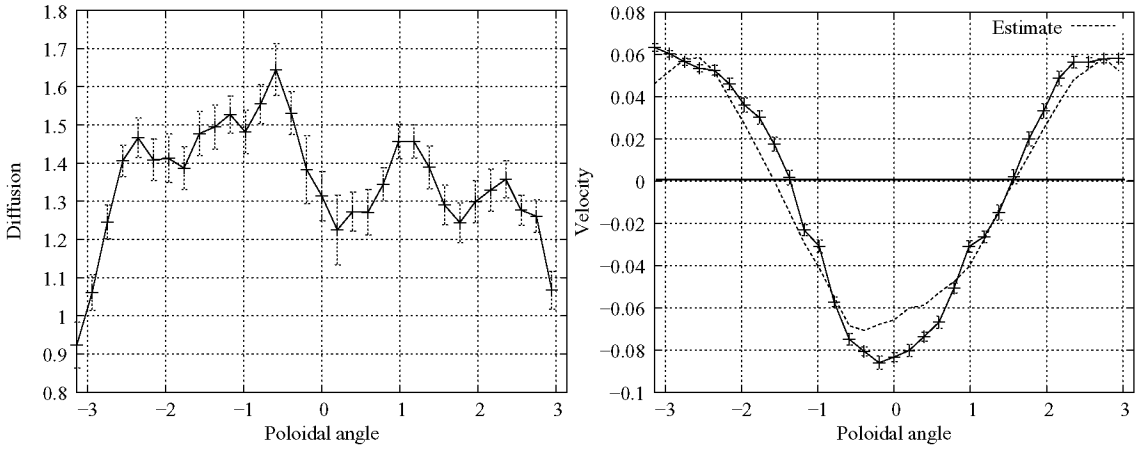

FIGURE 8. Impurity diffusion D (top) and pinch velocity V (bottom) over poloidal position (s) with error-bars. The pinch velocity is compared to $\omega_b * \cos(s) * D(s)$ (from [35]).

Turbulent EquiPartition (TEP) [36, 37], similar to the arguments in connection with Eq. 12 In the absence of parallel convection, finite mass effects and diffusion, Eq. (**??**) has the following approximate Lagrangian invariant

$$L(s) = \ln n_{imp} + \omega_B cos(s)x - \omega_B sin(s)y \,, \tag{15}$$

where $\omega_B = 2\frac{L_\perp}{R}$ governing the toroidal magnetic field inhomogeneity, R is the tokamak major radius and $L_\perp$ the mean gradient length of the pressure profile. TEP assumes the spatial homogenization of L by the turbulence. Since the parallel transport is weak, each drift plane $s = const.$ homogenizes independently. This leads to profiles $< L(s) >_y = const(s)$. At the outboard midplane ($s = 0$) the impurities are effectively convected radially inward leading to an impurity profile ($< \ln n_{imp} >_y \propto const. - \omega_B x$), while at the high field side they are effectively convected outward ($< \ln n_{imp} >_y \propto const. + \omega_B x$). One should note that this effective inward or outward convection is not found as an average $E \times B$ velocity, but is mitigated by the effect of spatial homogenization of L under the action of the turbulence. The strength of the "pinch" effect is consequently proportional to the mixing properties of the turbulence and scales with the measured turbulent diffusion. We arrive at the following expression for the connection between pinch and diffusion:

$$V(s) = -\alpha \omega_B \cos(s) D(s) \,. \tag{16}$$

Considering a stationary case with zero flux and combining Eq. (15) and Eq. (13) we obtain $\alpha = 1$. The ballooning in the turbulence level causes the inward flow on the outboard midplane to be stronger than the effective outflow on the high-field side. Therefor, averaged over a flux surface and assuming poloidally constant impurity density, a net impurity inflow results. This net pinch is proportional to the diffusion coefficient D in agreement with experimental observations [38]. The proportionality constant will, however, depend on the amount of ballooning of the transport, which has been investigated f.x. in [39, 40, 34]. The level of ballooning of the transport increases with the transition from the drift regime to the MHD regime, as $\hat{\beta}$ increases to large values. Here, for small $\hat{\beta}$ the ballooning of the transport is weak at about 70%.

Inertial pinch

The equation for the impurities can be rewritten in the form [41]:

$$d_t(\ln\theta - \zeta\omega) = \zeta \nabla_\perp \ln\theta \cdot d_t \nabla_\perp \varphi + \frac{\mu_\theta}{\theta} \nabla_\perp^2 \theta \,. \tag{17}$$

If the diffusivity μ_θ is of order $\zeta \ll 1$ and fluctuations θ_1 of the impurity density measured relative to a constant impurity background θ_0 do not exceed a corresponding level, the quantity $\ln\theta - \zeta\omega$ is approximately a Lagrangian invariant. Turbulent mixing will homogenise Lagrangian invariants in TEP states [42, 37], leading to

$$\ln\theta - \zeta\omega \approx \text{const}, \tag{18}$$

which constitutes a prediction about the effect of compressibility on the initially homogeneous impurity density field. The conservation of impurity density yields

$$\frac{\theta}{\theta_0} \approx 1 + \zeta\omega, \tag{19}$$

which conforms with the assumed ordering. We thus predict a linear relation between impurity density θ and vorticity ω, the proportionality constant being the mass–charge ratio ζ. This is related to, but not the same as, the aggregation of dense particles in vortices in fluids due to the Coriolis force [43]. The prediction is verified by numerical simulations of inertial impurities in saturated HW-turbulence for $\mathscr{C} = 1$. The simulations are performed on a $[-20, 20]^2$ domain, using 512×512 gridpoints, and impurity diffusivity 0.02. The impurity density field is initially set to unity. The impurity density field for $\zeta = 0.01$ is presented together with vorticity in Figure 9. Figure 10 shows a scatter plot of the point values of impurity density and vorticity at time 150 for three different values of ζ. The proportionality factor $\theta = 1 + K\omega$ is determined to be slightly below one: $K \simeq 0.82\,\zeta$.

The role of inertia for a radially inward pinch is investigated by considering the collective drift of impurities.

$$\vec{\Gamma}_\theta \equiv \vec{\Gamma}_\theta^E + \vec{\Gamma}_\theta^p \equiv \int \vec{x}\theta \vec{\hat{z}} \times \nabla_\perp \varphi + \int \vec{x}\theta\, \zeta\, d_t \nabla_\perp \varphi, \tag{20}$$

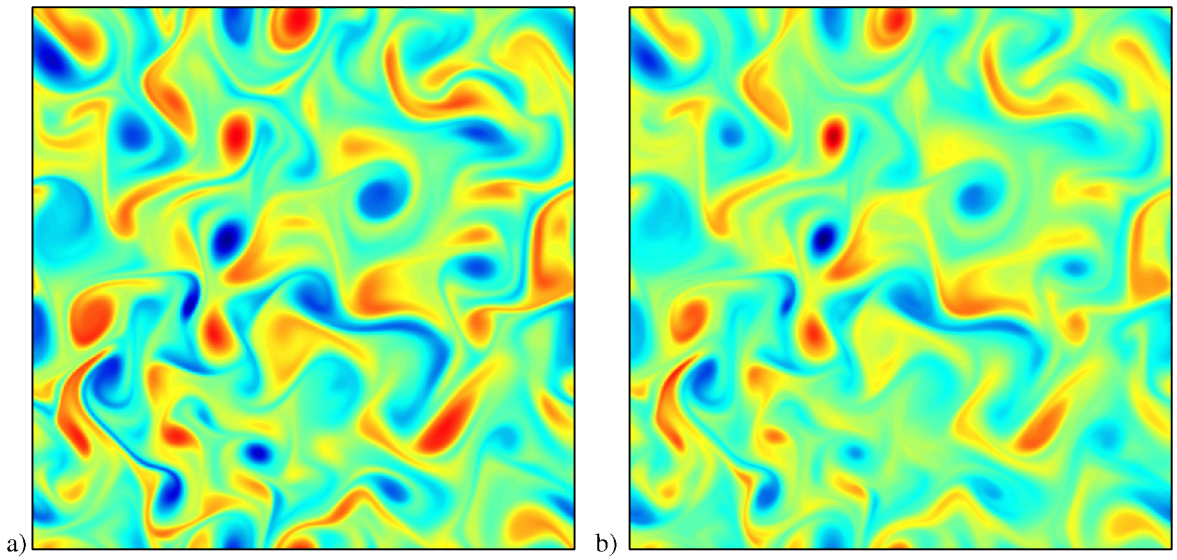

FIGURE 9. (a) Vorticity and (b) density of inertial impurities in the saturated state with $\mathscr{C} = 1$ and $\zeta = 0.01$, L = 40. Other parameters: $\mu_n = \mu_\omega = \mu_\theta = 0.02$.

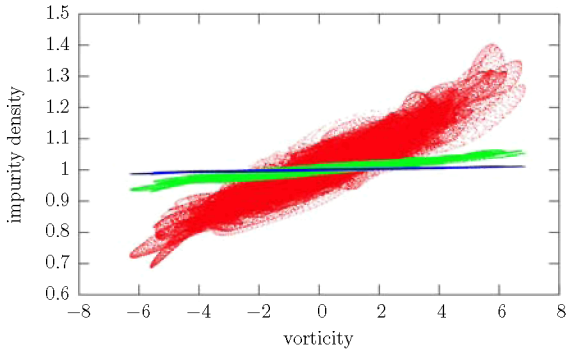

FIGURE 10. Scatter plot of impurity density and the vorticity field at $t = 100$ for different values of the mass–charge ratio ζ in the saturated state in HW with $\mathscr{C} = 1$: $\zeta = 0.05$ (red), $\zeta = 0.01$ (green), and $\zeta = 0.002$ (blue).

TABLE 1. Radial drift velocity of impurities for different values of the mass–charge ratio ζ in the saturated state in HW with $\mathscr{C} = 1$. Calculated as the average value between $t = 25$ and $t = 150$. Parameters: $\mu_n = \mu_\omega = \mu_\theta = 0.02$.

ζ	radial drift
−0.010	8.67×10^{-4}
0.001	-8.66×10^{-5}
0.002	-1.73×10^{-4}
0.005	-4.35×10^{-4}
0.010	-8.69×10^{-4}
0.020	-1.75×10^{-3}
0.050	-4.55×10^{-3}

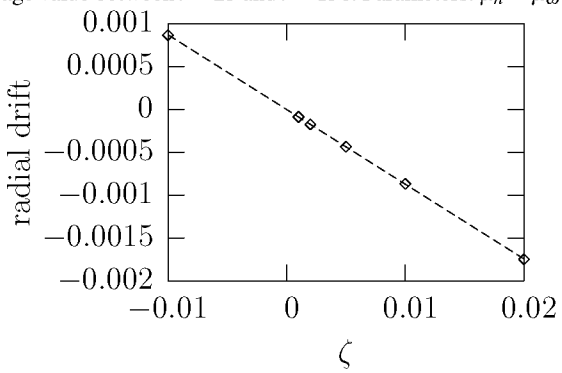

In terms of the integral impurity flux, we define an overall impurity drift velocity $\vec{V}_\theta$ by

$$\vec{V}_\theta \equiv \vec{V}_\theta^E + \vec{V}_\theta^p \equiv \frac{\vec{\Gamma}_\theta^E}{\int \vec{x}\theta} + \frac{\vec{\Gamma}_\theta^p}{\int \vec{x}\theta} = \frac{\vec{\Gamma}_\theta}{\int \vec{x}\theta}, \tag{21}$$

Ideal impurities do on average not experience a drift, but this is not the case for inertial impurities, since compressibility effects arrange for a correlation between θ_1 and ω. Note that only the deviations from the above discussed linear relationship $\theta = 1 + K\omega$ result in a net flow, as $\int K\omega v_r dx = 0$ for periodic boundary conditions. The radial drift velocity has a definite sign that depends on the sign of ζ, which was first discussed in [44]. There is a continuous flow of impurities in a definite direction (inward for positively charged impurities). This resembles the anomalous pinch observed in magnetic confinement experiments [45]. Average radial drift velocities computed using the values of the drift from $t = 25$ to $t = 150$ are presented in Table 1. The scaling of the average radial drift with ζ is seen to be remarkably linear.

Parallel compressibility pinch

A similar pinch effect results from compressibility along magnetic field lines, that is when parallel advection is taken into consideration, details can be found in [46].

Thermodiffusion

Additional pinch effects appear from off-diagonal elements of the transport matrix. Obviously this needs the introduction of a finite impurity temperature and thus a finite impurity pressure. To elucidate this effect we consider, for illustration only, the system of impurity pressure and density in a system with an effective curvature given via ω_B [47] :

$$d_t n_Z = -\omega_B \left(n_Z \nabla\phi + \frac{1}{Z}\nabla p_Z \right) \tag{22}$$

$$d_t p_Z = -\Gamma\omega_B \left(p_Z \nabla\phi + \frac{1}{Z}\nabla p_Z^2/n_Z \right) \tag{23}$$

with $\Gamma = 5/3$. We evaluate the quasilinear fluxes, assuming that the impurity density response is due to an external potential perturbation caused by some instability and arrive at the following expression for the particle ($Gamma_Z$) and heat (Q_Z) fluxes:

$$\begin{pmatrix} \frac{\Gamma_Z}{n_Z} \\ \frac{Q_Z}{n_Z T_Z} \end{pmatrix} = - \begin{bmatrix} D_n n & D_n T \\ D_n t & D_T T \end{bmatrix} \begin{pmatrix} \partial_r n_Z/n_Z + \omega_B \\ \partial_r T_Z/T_Z + \omega_B(\Gamma - 1) \end{pmatrix} \tag{24}$$

in which case we see that the quasilinear particle flux recovers the curvature pinch (occurence of $omega_B$), but through the off diagonal element picks up a contribution proportional to the gradient of the impurity temperature ($D_n T$). Expressing the flux now in terms of a diffusive contribution, namely everything that is proportional to ∇n_z and a pinch (the rest), this term leads to a pinch effect. The physics behind this easy, namely the plasma can increase entropy more efficiently by exchanging a larger number of colder impurity ions with a smaller number of hotter ions. The effective energy flux is down gradient in this case.

It should be noted, however, that in the quasilinear estimate the actual direction of the pinch effects (including thermodiffusion) depends on the propagation velocity of the underlying unstable modes.

QUASI–LINEAR GYROKINETIC CALCULATIONS OF IMPURITY TRANSPORT (AND COMPARISON WITH EXPERIMENTS)

Recently, the need of explaining and predicting impurity transport observations in fusion experiments which cannot be accounted for by neoclassical transport, lead to calculations of turbulent impurity transport adopting a physical description as realistic as possible, by the application of gyrokinetic models, and related codes.

In order to show how these calculations can be performed, first we recall that the δf gyrokinetic equation for the perturbed distribution function of particles of a given species is linear in the radial logarithmic gradients of the unperturbed (equilibrium) density and temperature of particles of the same species. Therefore, for small charge concentration of the impurity, which is usually the case for large part of the impurities in the experimental conditions, impurities should behave close to the passive (tracer) limit. In this case, a linear relationship holds between the particle flux of the impurity, and its density and temperature logarithmic gradients, which we express in terms of the dimensionless ratio of the major radius R to the gradient length L, namely

$$\frac{R\Gamma}{n_s} = D\frac{R}{L_{ns}} + D_T\frac{R}{L_T} + RV_P. \tag{25}$$

Here the diagonal diffusive coefficient D, the off-diagonal thermodiffusive coefficient D_T and the pure convection term V_p can be identified directly.

This property can be used in the framework of quasilinear gyrokinetic calculations in order to compute the previous contributions separately and measure the relative weight of each one and perform comparisons with the experiments. In experimental stationary conditions, in the absence of sources, the flux of the impurity is close to zero, which implies that for practical purposes it is useful to introduce the coefficients $C_T = D_T/D$ and $C_P = RV_P/D$. Then, the parameter $V/D \approx \frac{R}{L_{ns}}$ usually directly accessible in the experiments can be obtained by the sum of the thermodiffusive and pure convection contributions, in the form

$$\frac{RV}{D} = C_T\frac{R}{L_T} + C_P. \tag{26}$$

This quantity can be computed directly with a gyrokinetic code and compared to the experimental observations. Such investigations have been performed using the gyrokinetic code GS2 [48, 49]. As already presented in the previous section, it has been noted that the signs of the coefficients C_T and C_P may change depending on the direction of propagation of the background plasma microinstability [50, 46, 47, 51, 52]. In particular the thermodiffusive term provides an outward/inward contribution for modes propagating in the ion/electron diamagnetic direction [53, 50, 46], and decreases with increasing charge of the impurity, while the pure convection coefficient is usually directed inwards by E×B compression. Parallel dynamics adds a contribution to this term [46] which can lead to a total particle flux which is directed outwards, in the case of modes propagating in the electron diamagnetic direction. Conditions of outward impurity convection are extremely interesting from the experimental side, particularly in the development of ITER relevant scenarii. Therefore, some recent work has focused on the conditions for which an outward impurity convection is measured experimentally (e.g. [54, 55, 56]). Here we show specific gyrokinetic simulations of the previously introduced pure convection coefficient for the experimental conditions presented in Ref. [55]. In these experiments in ASDEX Upgrade (AUG), with Si laser ablation, a central outward total impurity convection was measured in the presence of strongly localized central electron cyclotron heating, while in the absence of this, the impurity convection was measured directed inwards. Such a transition in the behaviour cannot be explained by neoclassical transport. For this reason, corresponding investigations with a gyrokinetic model have been performed [52]. Input parameters of the gyrokinetic calculations were taken using experimental measurements. It has been found that in the plasma centre, in the presence of strong electron heating, producing locally strong electron temperature gradients, modes propagating in the electron diamagnetic direction can be destabilized. These modes feature an extremely elongated eigenfunction along the field line, shown in Fig. 11(a), and are generated by the non-adiabatic passing electron response of passing electrons. Passing electrons are transported inward in these conditions. Such an electrostatic potential develops an eleongated structure of parallel velocity fluctuations by parallel force balance, shown in Fig. 11(b). The latter, by parallel compression, leads to the development of a radial impurity flux which is directed outwards, as shown in Fig 11(c), for these modes, which have phase velocity in the electron diamagnetic direction. The mechanism of outward impurity convection introduced in Ref. [46] is found to occur in the specific simulation of these AUG experimental conditions. We mention also that such an outward convection mechanism is not specific exclusively of very long wave numbers, as erroneously pointed out in [51], but covers the full usual long wave length spectrum, as specifically demonstrated in [52]. We have to mention as well that the destabilization of these extremely elongated eigenfunctions is possible only in the very central region of the plasma, and that this kind of modes cannot be thought to be responsible of the outward convection observed at mid-radius in JET in Ni laser ablation experiments [56]. In that case, usual ballooning ITG modes were found as dominant modes, producing an inward convection of the impurity, in disagreement with the experimental observations. An outward impurity flux of the impurity was found in the gyrokinetic simulations of these experiments only by switching off the ITG instability and singling out the effect of the otherwise subdominant trapped electron mode.

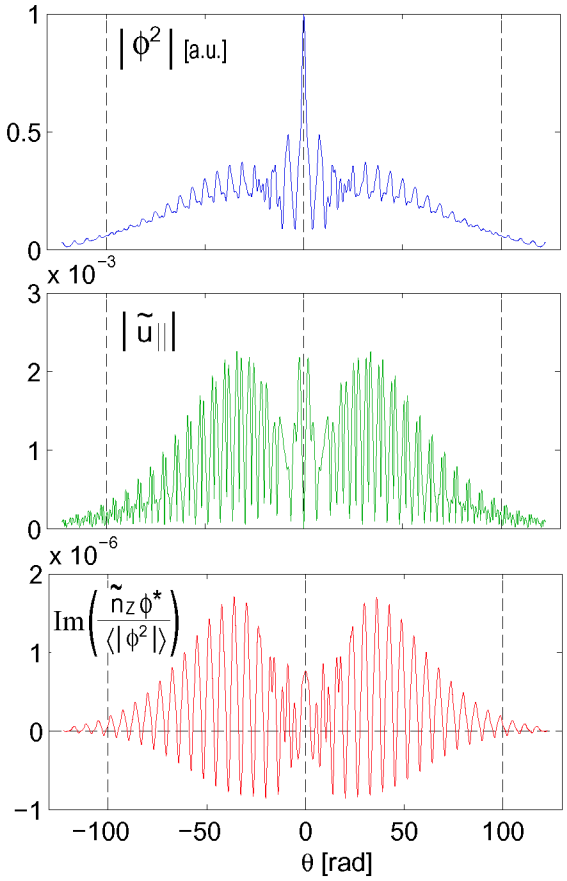

FIGURE 11. Linear mode structure along the field line of the electrostatic potential fluctuations $|\phi^2|$ (a), of the Si parallel velocity $|\tilde{u}|$ (b), and of the normalized cross phase relationship between Si denity fluctuations and electrostatic potential fluctuations, proportional to the Si radial flux, (c) as a function of the extended ballooning angle θ for a calculation with experimental input parameters for a AUG H–mode plasma with central electron heating [52].

In conclusion, the study of turbulent impurity transport by means of gyrokinetic models has made significant progresses and first non-trivial qualitative agreement between the experimental observations and the theoretical predictions have been found. However, the way is still long before a model for impurity transport is indeed assessed for reliable ITER prediction purposes.

ACKNOWLEDGMENTS

One of the authors (VN) would like to acknowledge discussions with X. Garbet and Y. Yankov on pinch effects and thermodiffusion.

REFERENCES

1. A. Kallenbach, R. Neu, R. Dux, H. Fahrbach, J. Fuchs, L. Giannone, O. Gruber, A. Herrmann, P. Lang, B. Lipschultz, C. Maggi, J. Neuhauser, V. Philipps, T. Putterich, V. Rohde, J. Roth, G. Sergienko, A. Sips, and ASDEX Upgrade Team, *Plasma Phys. Controlled Fusion* **47**, B207–B222 (2005).
2. S. P. Hirshman, and D. J. Sigmar, *Neoclassical transport of impurities in Tokamak plasmas*, Unknown, 1981.
3. H. Tennekes, and J. L. Lumley, *A First Course in Turbulence*, MIT Press, Cambridge, Massachusetts, 1972, ISBN 0-262-20019-8.
4. W. D. McComb, *The Physics of Fluid Turbulence*, Clarendon Press, Oxford, 1990.

5. D. Elhmaïdi, A. Provenzale, and A. Babiano, *J. Fluid Mech.* **257**, 553–558 (1993).
6. A. Provenzale, *Annu. Rev. Fluid. Mech.* **31**, 55–93 (1999).
7. C. Pasquero, A. Provenzale, and A. Babiano, *J. Fluid Mech.* **439**, 279–303 (2001).
8. A. V. Milovanov, *Phys. Rev. E* **63**, 047301 (2001).
9. G. M. Zaslavsky, *Phys. Rep.* **371**, 461 – 580 (2002).
10. J. Lynov, A. Nielsen, H. Pécseli, and J. Rasmussen, *J. Fluid Mech.* **224**, 485–505 (1991).
11. J. H. Misguich, R. Balescu, H. Pécseli, T. Mikkelsen, S. Larsen, and Q. Xiaoming, *Plasma Phys. and Contr. Fusion* **29**, 825–856. (1987).
12. M. Pettini, A. Vulpiani, J. H. Misguich, M. D. Leener, J. Orban, and R. Balescu, *Phys. Rev. A* **38**, 344–363 (1988).
13. M. Vlad, F. Spineanu, J. H. Misguich, and R. Balescu, *Phys. Rev. E* **58**, 7359–7368 (1998).
14. R. Balescu, *Aspects of Anomalous Transport in Plasmas*, Taylor and Francis Group, CRC Press, Paris, 2005.
15. A. Hasegawa, and M. Wakatani, *Phys. Rev. Lett.* **50**, 682–686 (1983).
16. V. Naulin, A. H. Nielsen, and J. Juul Rasmussen, *Phys. Plasmas* **6**, 4575 – 4585 (1999).
17. R. Basu, T. Jessen, V. Naulin, and J. Juul Rasmussen, *Phys. Plasmas* **10**, 2696–2703 (2003).
18. R. Basu, V. Naulin, and J. Juul Rasmussen, *Comm. in Nonlinear Science and Numerical Simulation* **8**, 477–492 (2003).
19. G. Manfredi, and R. O. Dendy, *Phys. Rev. Lett.* **76**, 4360 (1996).
20. B. Krane, H. L. Pécseli, and J. Trulsen, *Phys. Fluids* **15**, 211–226 (2003).
21. M. Vlad, F. Spineanu, S. I. Itoh, M. Yagi, and K. Itoh, *Plasma Phys. Controlled Fusion* **47**, 1015–1029 (2005).
22. T. Hauff, and F. Jenko, *Phys. Plasmas* **13**, 102309 (2006).
23. T. Hauff, and F. Jenko, *Phys. Plasmas* **14**, 092301 (2007).
24. S. Guenter, G. Conway, S. DaGraca, H.-U. Fahrbach, C. Forest, M. Munoz, T. Hauff, J. Hobirk, V. Igochine, F. Jenko, K. Lackner, P. Lauber, P. McCarthy, M. Maraschek, P. Martin, E. Poli, K. Sassenberg, E. Strumberger, G. Tardini, E. Wolfrum, H. Zohm, and Asdex Upgrade Team, *Nucl. Fusion* **47**, 920–928 (2007).
25. S. V.Annibaldi, G. Manfredi, R. Dendy, and L. Drury, *Plasma Phys. Controlled Fusion* **42**, L13–L22 (2000).
26. S. V.Annibaldi, G. Manfredi, and R. Dendy, *Phys. Plasmas* **9**, 791–799 (2002).
27. T. Huld, A. H. Nielsen, H. L. Pécseli, and J. J. Rasmussen, *Phys. Fluids B* **3**, 1609 – 1625 (1991).
28. M. Endler, H. Niedermeyer, L. Giannone, E. Holzauer, A. Rudyj, G. Theimer, N. Tsois, and Asdex-Team, *Nucl. Fusion* **35**, 1307–1339 (1995).
29. B. A. Carreras, C. Hidalgo, E. Sánchez, M. Pedrosa, R. Balbín, García-Cortés, B. van Milligen, D. E. Newman, and V. E. Lynch, *Phys. Plasmas* **3**, 2664–2672 (1996).
30. V. Naulin, and K. H. Spatschek, *Phys. Rev. E* **55**, 5883–5893 (1997).
31. M. B. Isichenko, and N. V. Petviashvili, *Phys. Plasmas* **2**, 3650–3654 (1995), URL `http://link.aip.org/link/?PHP/2/3650/1`.
32. O. E. Garcia, V. Naulin, A. H. Nielsen, and J. Juul Rasmussen, *Phys. Plasmas* **12**, 062309 (2005).
33. O. E. G. V. Naulin, A. H. Nielsen, and J. J. Rasmussen, *Physics AUC* **17**, 263 (2007).
34. V. Naulin, *Phys. Plasmas* **10**, 4016–4028 (2003).
35. V. Naulin, *Phys. Rev. E* **71**, 015402 R (2005).
36. J. Nycander, and V. V. Yankov, *Phys. Plasmas* **2**, 2874–2876 (1995).
37. V. Naulin, J. Nycander, and J. Juul Rasmussen, *Phys. Rev. Lett.* **81**, 4148 – 4151 (1998).
38. M. E. Perry, N. H. Brooks, D. A. Content, R. A. Hulse, M. ali Mahdavi, and H. W. Moos, *Nucl. Fusion* **31**, 1859 – 1874 (1991).
39. B. D. Scott, *Plasma Phys. Control. Fusion* **39**, 471 – 504 (1997).
40. B. D. Scott, *Plasma Phys. Control. Fusion* **39**, 1635 – 1668 (1997).
41. M. Priego, O. E. Garcia, V. Naulin, and J. Juul Rasmussen, *Phys. Plasmas* **12**, 062312.1–062312.11 (2005).
42. V. V. Yankov, *Physics-Uspekhi* **40**, 477–493 (1997).
43. A. Bracco, P. H. Chavanis, A. Provenzale, and E. A. Spiegel, *Phys. Fluids* **11**, 2280–2287 (1999).
44. V. Naulin, J. Juul Rasmussen, and M. P. Wood, "Pinch effects in turbulent impurity transport," in *Theory of Fusion Plasmas*, edited by J. W. Connor, O. Sauter, and E. Sindoni, Editrice Compositori, Bologna, 2004, pp. 365–371.
45. R. Dux, *Fusion Science and Technology* **44**, 708 – 715 (2003).
46. C. Angioni, and A. Peeters, *Phys. Rev. Lett.* **96**, 095003 (2006).
47. N. Dubuit, X. Garbet, T. Parisot, R. Guirlet, and C. Bourdelle, *Phys. Plasmas* **14**, 042301 (2007).
48. M. Kotschenreuther, G. Rewoldt, and W. Tang, *Computer Phys. Comm.* **88**, 128 (1995).
49. W. Dorland, F. Jenko, M. Kotschenreuther, and B. Rogers, *Phys. Rev. Lett.* **85**, 5579 (2000).
50. X. Garbet, N. Dubuit, E. Asp, Y. Sarazin, C. Bourdelle, P. Ghendrih, and G. Hoang, *Phys. Plasmas* **12**, 082511 (2005).
51. C. Bourdelle, X. Garbet, F. I. andA. Casati, N. Dubuit, R. Guirlet, and T. Parisot, *Phys. Plasmas* **14**, 112501 (2007).
52. C. Angioni, R. Dux, E. Fable, and A. G. Peeters, *Plasma Phys. Controlled Fusion* **49**, 2027 (2007).
53. M. Frojdh, Liljestrom, and H. Nordman, *Nucl. Fusion* **32**, 419 (1992).
54. E. Scavino, J. Bakos, and H. Weisen, *Plasma Phys. Controlled Fusion* **46**, 857 (2004).
55. R. Dux, R. Neu, A. Peeters, G. Pereverzev, F. R. A. Mück, and J. Stober, *Plasma Phys. Controlled Fusion* **45**, 1815 (2003).
56. M. Puiatti, M. Valisa, C. Angioni, L. Garzotti, P. Mantica, M. Mattioli, L. Carraro, I. Coffey, and C. Sozzi, *Phys. Plasmas* **13**, 042501 (2006).